A Combined Theoretical and Experimental Study of Solid Octyl and Decylammonium Chlorides and of Their Aqueous Solutions

ARTICLE *in* THE JOURNAL OF PHYSICAL CHEMISTRY B · JUNE 2013

Impact Factor: 3.3 · DOI: 10.1021/jp403103w · Source: PubMed

THE JOURNAL OF PHYSICAL CHEMISTRY B

Article

pubs.acs.org/JPCB

A Combined Theoretical and Experimental Study of Solid Octyl and Decylammonium Chlorides and of Their Aqueous Solutions

Valentina Migliorati,*[,†] Paolo Ballirano,*[,‡] Lorenzo Gontrani,[§] Stefano Materazzi,[†] Francesca Ceccacci,[†] and Ruggero Caminiti[†]

[†]Dipartimento di Chimica, Università di Roma "La Sapienza", Piazzale Aldo Moro 5, 00185 Roma, Italy

[‡]Dipartimento di Scienze della Terra, Università di Roma "La Sapienza", Piazzale Aldo Moro 5, 00185 Roma, Italy

[§]Consiglio Nazionale delle Ricerche, Istituto di Struttura della Materia, Tor Vergata Via del Fosso del Cavaliere 100, 00133 Roma, Italy

ABSTRACT: The analysis of the thermal behavior of octyl- (OAC) and decylammonium chloride (DAC) has provided relevant new information. OAC shows a polymorphic phase transition that starts at 308 K and is completed at 313 K, between a monoclinic and a tetragonal structure, which belongs to a space group different from what was observed for other alkylammonium chlorides. At the melting temperature (463 K), the growing of a strong first sharp diffraction peak (FSDP) occurring at a *d*-spacing of ca. 21.0 Å was observed. DAC is characterized by two phase transitions at 318 (T_{d1}) and 323 K (T_{d2}). At T_{d1}, the LT polymorph coexists with a new-formed phase. At T_{d2} the LT polymorph is replaced by a further polymorphic modification of DAC that becomes the only one at 328 K. This second phase transition signals the occurrence of a phase, closely related to the LT polymorph of HeAC, that crystallizes in the tetragonal crystal system a = ca. 5.00 Å and c = ca. 28.5 Å, $P4/nmm$ space group. DAC melting starts at 458 K and is accompanied, as in the case of OAC, by the growing of a strong FSDP at a *d*-spacing of ca. 24.8 Å. A parallel DSC study confirmed the above-mentioned transitions. In addition, the structural properties of OAC/water and DAC/water mixtures were studied using an integrated approach, which combines X-ray diffraction and molecular dynamics (MD) techniques. A very good agreement between theoretical and experimental diffraction patterns has been obtained for both investigated mixtures. A thorough analysis of the MD trajectories shows that strong anion−water interactions are present in the mixtures, where Cl^- forms a rather unstructured first hydration shell of water molecules bound to the anion in a linear Cl···H−O configuration. Moreover, cations and anions were found to interact with each other, and to form "solvent-shared ion pairs", in which one or more water molecules are shared between Cl^- and the alkylammonium cation.

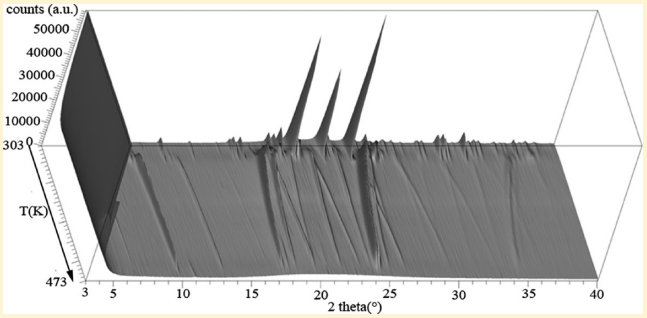

INTRODUCTION

Molten salts, as well as room temperature ionic liquids, are materials composed uniquely of oppositely charged species. The character of these species varies from classical ions in typical molten salts (fused alkali halides) to charged polyatomic molecules in ionic liquids. The prototype of molten salts are fused alkali halides that contain alkali and halogen ions and which exhibit high melting temperatures around 1000 K. On the other hand, most ionic liquids have a polyatomic organic cation and an inorganic or organic anion. They typically melt near room temperature and, therefore, are also named room temperature or ambient temperature molten salts. Both molten salts and ionic liquids possess a series of remarkable properties that have attracted the attention of the research community for academic and applicative issues and have been thoroughly studied both experimentally[1−3] and computationally.[3,4]

Alkylammonium chlorides are a family of molten salts that have found wide application, for example, in electrochemistry as supporting electrolytes and as reagents in organic and analytical chemistry.[5,6] Nowadays, a deep molecular level characterization of the complex network of interactions occurring in alkylammonium chlorides is still lacking, and, in this framework, we have recently undertaken a broad investigation of this class of materials, by using an integrated approach that combines high-temperature X-ray powder diffraction, X-ray diffraction measurements, and classical molecular dynamics (MD) simulations.[7−9] In particular, we have studied the crystal polymorphism of two of the shortest homologues of the family of monosubstituted alkylammonium chlorides, namely ethylammonium chloride (EAC),[7] propylammonium chloride (PAC),[8] and of hexylammonium chloride (HeAC),[9] and we have investigated the structural properties of EAC/water, PAC/water, and HeAC/water mixtures.[7−9]

Received: March 29, 2013
Revised: June 3, 2013
Published: June 3, 2013

In this paper we continue our broad investigation on the crystal polymorphism of alkylammonium chlorides and of their structural properties in mixtures with water, by focusing our attention on two alkylammonium chlorides with longer alkyl chain, namely, octylammonium chloride (OAC) and decylammonium chloride (DAC). Coherently, this study will be carried out by combining high-temperature X-ray powder diffraction, MD simulations, and energy-dispersive X-ray diffraction experiments, since this integrated approach has been found to be essential to gain reliable structural information on these systems. In addition, a parallel solid-state characterization by differential scanning calorimetry (DSC) is performed to support the study with thermoanalitical data in the same temperature range. The calorimetric profiles will be used to confirm the occurrence of polymorphic phase transitions and melting processes. A similar study was reported in 1968 by Tsau and Gilson,[10] but the calculated enthalpies were not accurate.

As far as the crystal polymorphism of OAC and DAC is concerned, the room-temperature (RT) structure of OAC has been reported to be monoclinic with the longest spacing of 25.4 Å.[11] This RT structure, referred to as secondary monoclinic phase, has been obtained by cooling from the high-temperature (HT) polymorph. A further primary monoclinic/orthorhombic phase has been proposed for *n*-alkylammonium chlorides for crystals that have not received thermal treatment. It is characterized by a halved longest spacing as compared to that of the corresponding secondary phase.[11] No such primary phase has been observed for OAC.[11] The HT structure of OAC (T > 333 K) has been reported to be equivalent to the RT-phase tetragonal of HeAC, space group $P4/nmm$.[11,12]

The RT structure of DAC is monoclinic, space group $P2_1$, a = 5.6996(4) Å, b = 7.1638(5) Å, c = 15.490(1) Å, β = 91.297(5)°.[13] The structure contains polar layers, consisting of NH_3 groups and chlorine atoms, alternating with neutral layers consisting of aliphatic chains. The layers are held together by van der Waals interactions. The chlorine and nitrogen atoms are linked by a hydrogen bond forming a two-dimensional (2D) honeycomb net. Two overlapping first-order phase transitions occurring between 315 and 333 K have been reported and attributed to a reconstructive transformation to a nonintercalated structure.[14]

EXPERIMENTAL SECTION

Preparation of the Alkylammonium Chlorides. Solvents (LC-MS grade) 1-aminodecane and 1-aminoottane (99%) were purchased from Aldrich. Chloridric acid (37% w/w) was purchased from Carlo Erba.

^{1}H and ^{13}C NMR spectra were recorded on a Bruker Avance 400 spectrometer, operating at 400.13 and 100.6 MHz, respectively; δ in ppm relative to the residual proton signal of deuterated solvent, J in Hz.

General Procedure for the Preparation of the Alkylammonium Chlorides.[15] To a solution of HCl (37%, 6.0 mL, 72 mmol) in 30 mL of EtOH, the amine (13 mmol) was slowly added under efficient stirring at room temperature. After one hour stirring, the solution was concentrated to obtain a white paste that was purified by crystallization.

OAC (White Crystals, Crystallized from EtOH/tBuOMe, 74%). ^{1}H NMR(DMSO-d_6): 8.15 (s, 3H, NH_3), 2.72 (*pt*, 2H, 7.2 Hz, CH_2N), 1.56 (*quin*, 2H, 7.2 Hz, CH_2CH_2N), 1.38−1.16 (*om*, 10H), 0.86 (*t*, 3H, 6.8 Hz, CH_3). ^{13}C NMR (DMSO-d_6): 38.6, 31.1, 28.5, 28.5, 26.9, 25.9, 22.1, 13.9. $C_8H_{20}ClN$: Calcd. C 57.99; H 12.17; N 8.45. Found: C 57.59; H 12.55; N 8.45.

DAC (White Crystals, Crystallized from EtOH/tBuOMe, 81%). ^{1}H NMR(DMSO-d_6): 8.07 (s, 3H, NH_3), 2.82−2.60 (*m*, 2H, CH_2N), 1.54 (*quin*, 2H, 7.4 Hz, CH_2CH_2N), 1.35−1.10 (*om*, 14H), 0.85 (*t*, 3H, 6.8 Hz, $C\underline{H}_3$).^{13}C NMR (DMSO-d_6): 38.6, 31.3, 28.9, 28.8, 28.7, 28.5, 26.8, 25. 9, 22.0, 13.9. $C_{10}H_{24}ClN$: Calcd. C 61.99; H 12.48; N 7.23. Found: C 61.60; H 12.85; N 7.17.

High-Temperature X-ray Powder Diffraction (HT-XRPD) measurements. Powders of the title compounds were loaded and packed in 1.0 mm diameter silica-glass capillaries open at one end. The samples were used without any further purification. Diffraction data were collected on a parallel-beam Bruker AXS D8 Advance, operating in transmission in $\theta-\theta$ geometry. The instrument is fitted with a PSD VÅNTEC-1 detector set to a 6° 2θ aperture and with a prototype of capillary heating chamber.[16−19] Isothermal measurements were carried out from 303 K up to melting. Details of data collection are reported in Table 1. A magnified view of the complete data sets of OAC and DAC is shown in Figure 1. A second sample of OAC was prepared, and a new measurement was replicated using the same experimental conditions used for the first sample. This procedure was adopted in order to test the possible influence of different relative humidity conditions on the thermal stability of the sample. Because a preliminary scrutiny of the diffraction patterns of OAC indicated the occurrence of a discontinuity at 308 K, two further diffraction patterns were measured at 295 and 297 K.

Table 1. Details of HT-XRPD Data Measurements

	OAC		DAC
	I run	II run	
angular range (°2θ)		3−90	
step size (°2θ)		0.0219	
counting time (s)		3	
thermal range (K)	303−493	303−523	303−473
temperature steps (K)		5	
number of patterns	39	47	35
radiation		Cu-K_α	

Energy Dispersive X-ray Scattering Measurements. OAC and DAC were dried in vacuum for about 48 h. The OAC/water and DAC/water mixtures were then prepared by mixing weighed amounts of freshly distilled water and of the solid compound, thus obtaining OAC/water and DAC/water molar ratios of 1:101.7 and 1:91.5 and experimental densities of 1.05 and 0.945 g/cm^3, respectively. The samples were rapidly transferred into a sealed cell with Mylar windows. Sample and windows thicknesses were 3 mm and 6 μm, respectively. The large angle X-ray scattering (LAXS) experiments were conducted using the noncommercial energy-scanning diffractometer[20,21] built in the Chemistry Department of the Rome University "La Sapienza". Data treatment, as well as the protocol to obtain structure functions $I(Q)$ and radial distribution functions Diff(r) are analogous to what was reported in refs 7−9.

Molecular Dynamics Simulation Details. The MD simulations of the OAC/water and DAC/water mixtures were carried out using the DL_POLY package.[22] The systems were composed by 27 ion pairs and 2745 water molecules placed in a

dx.doi.org/10.1021/jp403103w | J. Phys. Chem. B 2013, 117, 7806−7818

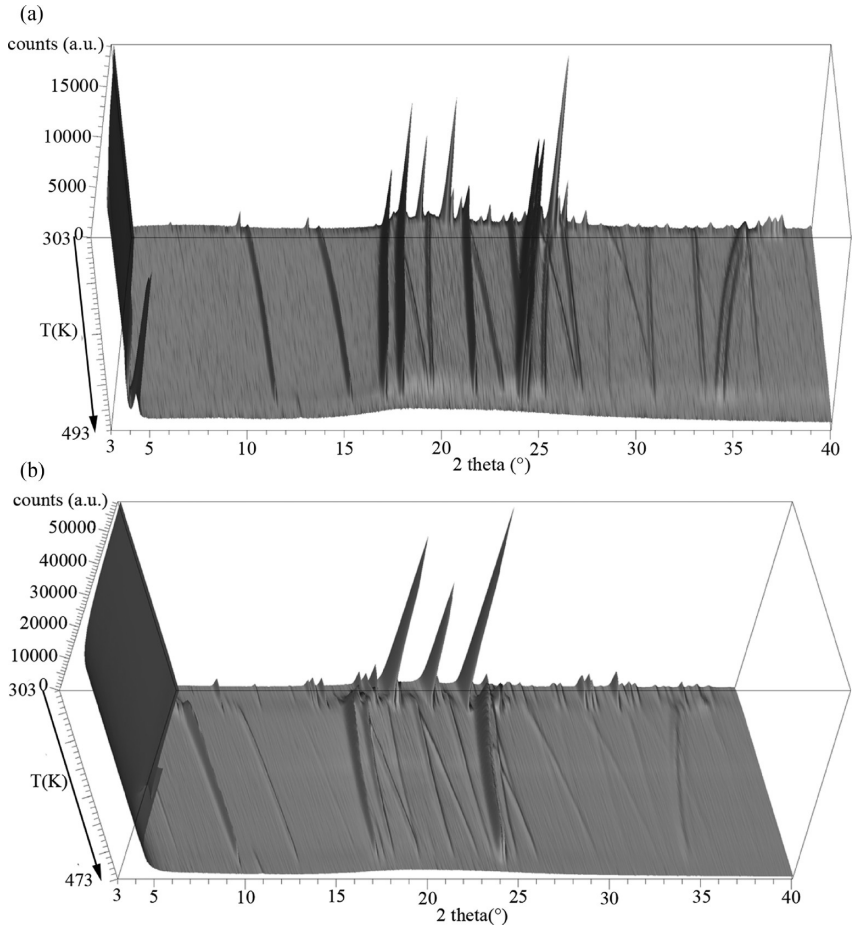

Figure 1. Magnified view of the full data set of the heating cycle of (a) OAC II run and (b) DAC.

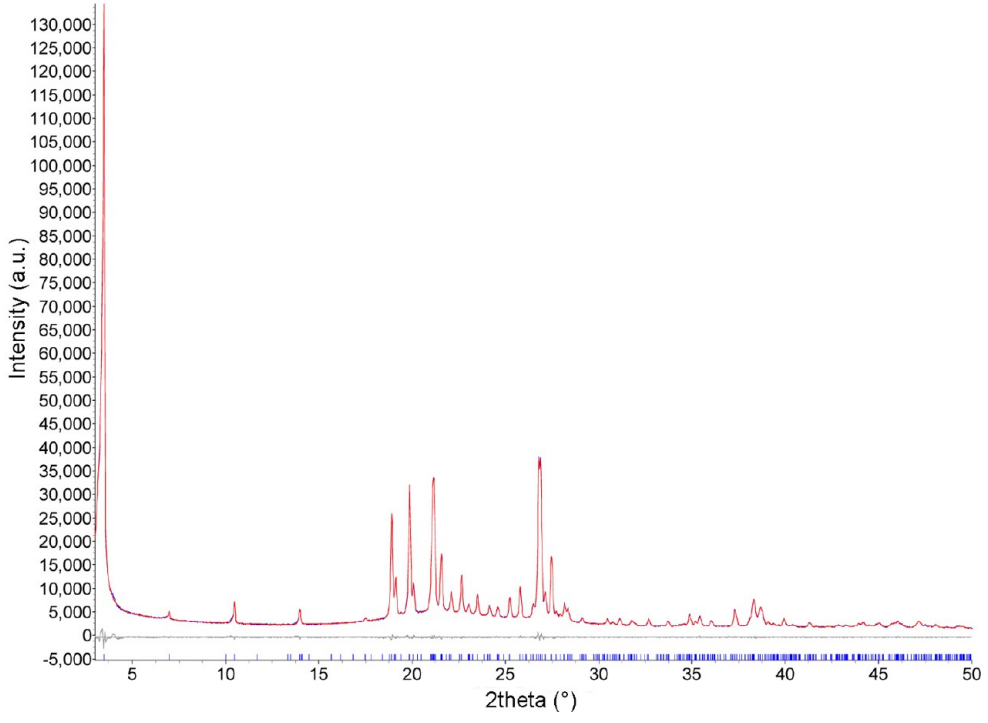

Figure 2. LeBail fitting of the diffraction data collected at 295 K using the proposed monoclinic unit cell. Blue: experimental; red: calculated; below: difference.

dx.doi.org/10.1021/jp403103w | J. Phys. Chem. B 2013, 117, 7806−7818

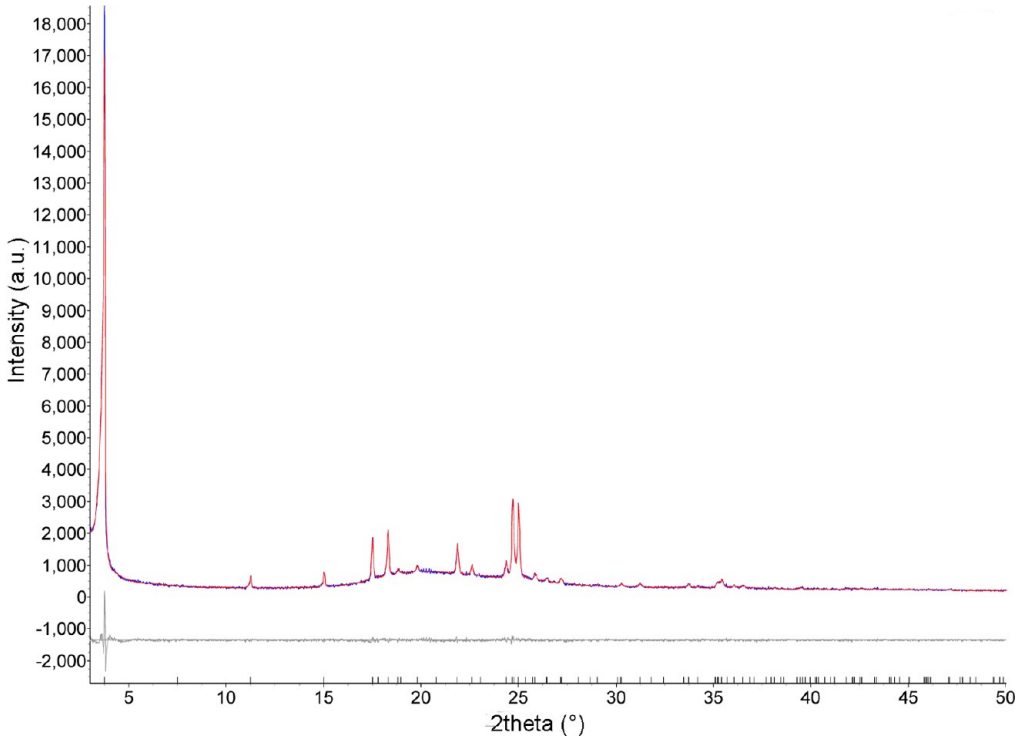

Figure 3. LeBail fitting of the diffraction data collected at 373 K using the proposed tetragonal unit cell. Blue: experimental; red: calculated; below: difference.

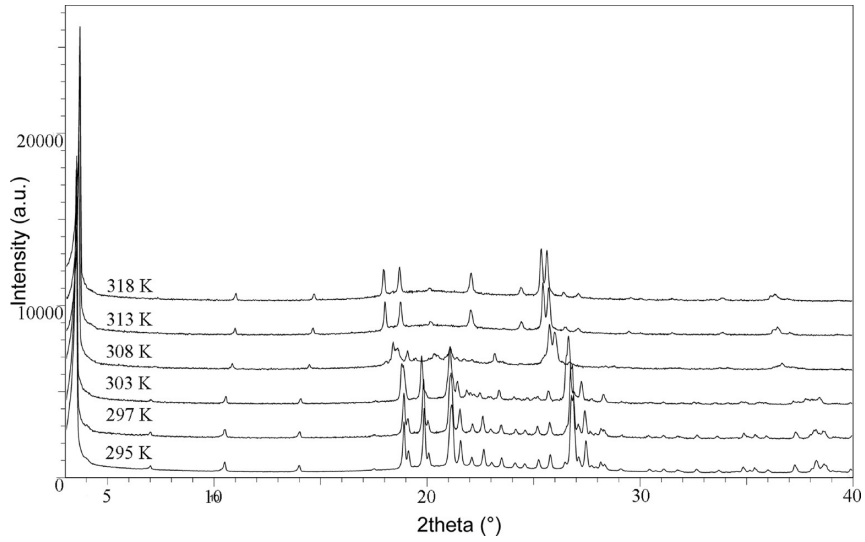

Figure 4. Magnified view of the diffraction patterns of OAC measured in the 295 K ≤ T ≤ 318 K thermal range.

cubic box of 44.07 Å edge for OAC, while 27 ion pairs and 2471 water molecules were simulated in the case of DAC in a cubic box with an edge length of 44.35 Å. Note that the OAC/water and DAC/water molar ratios of the simulated systems were the same of those used in the experiments, and the sizes of the simulation boxes were chosen to reproduce the experimental densities of the systems under investigation.

For the partial charges of the cation we used the OPLS-AA charges for ammonium ions,[23] while all of the other force field parameters for the OAC and DAC ion were taken from the Lopes and Padua force field.[24,25] For water, one of the most widespread water models was employed, namely, the TIP5P,[26] which is a five-site model in which the oxygen is neutral and the negative charge is placed on two massless dummy atoms located orthogonal to the water plane. The Lennard-Jones parameters for all of the unlike atoms were obtained from the Lorentz−Berthelot combining rules with the exception of one Lennard-Jones parameter for the Cl−water interaction ($\sigma_{Cl\text{-}OW}$), for which the value previously optimized for the EAC/water mixture was used.[7]

For further MD simulation protocol details, theoretical diffraction functions definition[27] as well as for the details in the comparison between experimental and simulation data, the reader is referred to refs 7−9.

Angular distribution functions were computed from MD simulations for two different angles: the angle formed by two

dx.doi.org/10.1021/jp403103w | J. Phys. Chem. B 2013, 117, 7806−7818

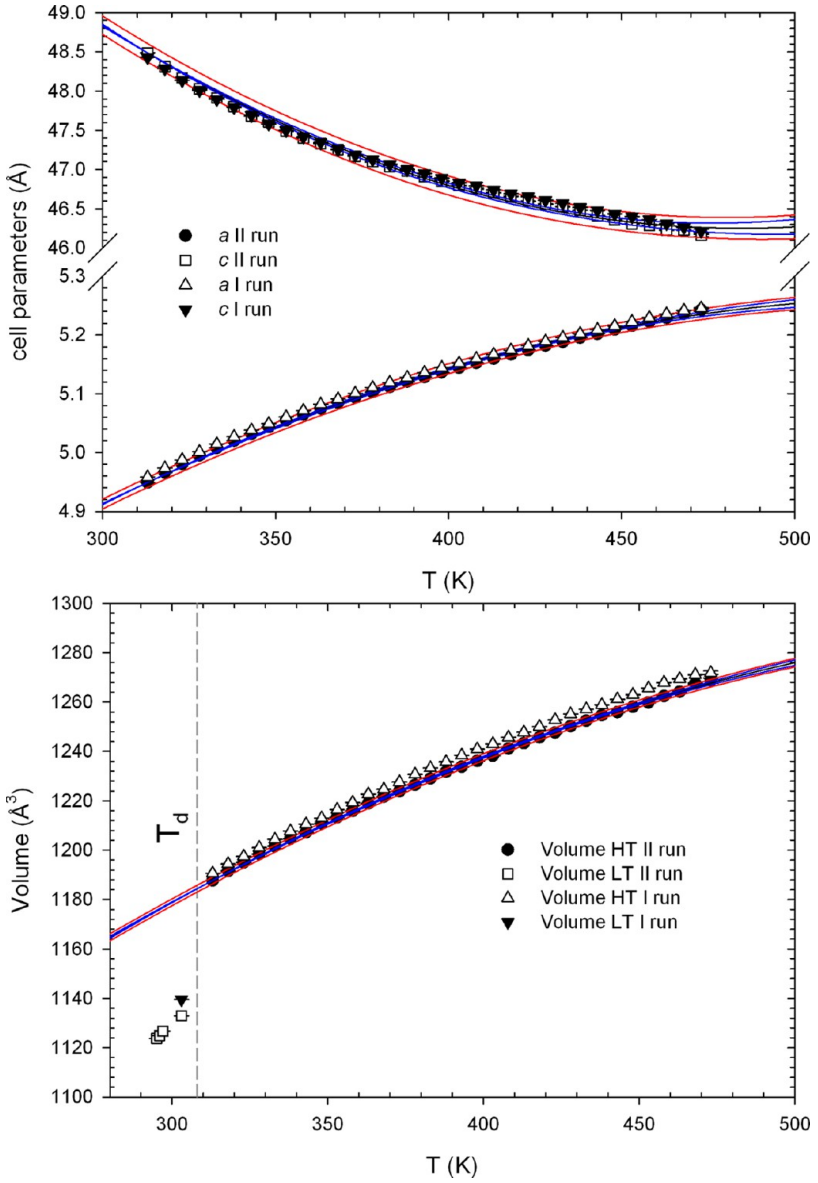

Figure 5. Evolution of cell parameters and volume with temperature of HT-OAC: (a) *a* and *c* cell parameters; (b) volume. Fitting of the expression $\alpha_V(T) = a_0 + a_1T$ (see below), confidence (95% level), and prediction intervals are reported for the II run. Vertical dashed gray line indicates the temperature T_d at which the polymorphic transformation LT-OAC → HT-OAC has been observed.

Cl−O vectors (labeled as ψ) and the angle formed by the Cl−O and O−H vectors (labeled as ω), where O and H are the oxygen and hydrogen atoms of the water molecules in the first hydration shell of the Cl^- ion. All MD analyses were carried out using in-house written codes.

DSC Characterization. The DSC curves were obtained by heating a few milligrams of each sample under the following experimental conditions: instrument Perkin-Elmer DSC7, sealed aluminum pans, sample weight average 10 mg, heating rate 2 K min^{-1}, and temperature range 283−513 K.

RESULTS AND DISCUSSION

Crystal Polymorphism of OAC. The two data sets show exclusively marginal differences related to a minor (ca. 1 K) temperature offset, due to recalibration of the thermocouple between the two measurements. The following discussion will be focused on the first data set.

The starting of a phase transition has been detected at 308 K signaled by an increase of the background and by severe modifications of the diffraction pattern. The conversion is completed at 313 K. No further structural modifications were observed up to the melting temperature.

As far as the LT (T < 308 K) structural modification is concerned, autoindexing was performed on the pattern measured at 295 K using the LSI algorithm,[28] implemented in Topas 4.2,[29] which is based on an iterative use of least-squares. A solution was obtained in the monoclinic system for the following cell parameters a = 25.5771(4) Å, b = 4.72090(5) Å, c = 9.39663(10) Å, β = 97.8549(15)°, volume 1123.97(6) Å^3, Z = 4. Analysis of the reflection conditions *h*0*l* and 00*l* with $l = 2n$, and 0*k*0 with $k = 2n$, indicates $P2_1/c$ as the possible space group. A LeBail fitting of the diffraction data confirmed the correctness of the proposed unit cell (Figure 2).

Due to the possible occurrence of anisotropic thermal expansion, the HT data were carefully checked in order to find

dx.doi.org/10.1021/jp403103w | J. Phys. Chem. B 2013, 117, 7806−7818

Table 2. Linear and Volume Thermal Expansion Coefficients a_0 and a_1 of HT-OAC[a]

		OAC
		308 K < T < 473 K
a-parameter	R^2	0.9978
	$a_0(x\ 10^{-6})$	554(4)
	$a_1\ (x\ 10^{-8})$	−120(5)
	a_{Tr}	4.94927(14)
c-parameter	R^2	0.9927
	$a_0(x\ 10^{-6})$	−537(9)
	$a_1\ (x\ 10^{-8})$	156(7)
	c_{Tr}	48.488(3)
V	R^2	0.9993
	$a_0(x\ 10^{-6})$	559(4)
	$a_1\ (x\ 10^{-8})$	−86(3)
	V_{Tr}	1187.72(10)

[a]They were obtained by fitting the data to the expression $\alpha_V(T) = a_0 + a_1T$. a_{Tr}, c_{Tr}, and V_{Tr} are the a-parameter, c-parameter, and volume at reference temperature T_r = 313 K. R^2 = determination coefficients.

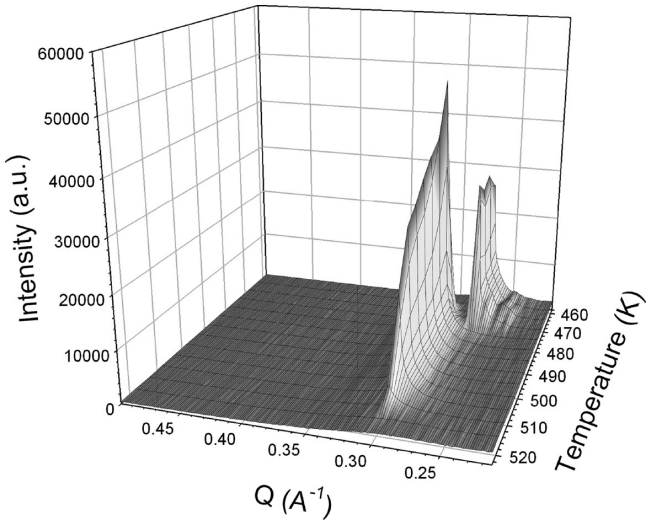

Figure 6. Evolution of FSDP of OAC, located at Q ca. 0.30 Å^{-1}, from 463 to 523 K.

a temperature at which the largest number of nonoverlapped peaks was accessible. Such condition was met by the diffraction pattern collected at 378 K. Indexing of the patterns was performed following the same procedure of the LT polymorph. A solution was obtained in the tetragonal system for the following cell parameters a = 5.10074(6) Å, c = 47.1860(22) Å, volume 1227.67(6) Å^3, Z = 4. Analysis of the reflection conditions $hk0$ with $h+k = 2n$, $00l$ with $l = 2n$, and $0k0$ with $k = 2n$, points out to $P4_2/n$ as the possible space group. The corresponding LeBail fitting is shown in Figure 3.

Therefore, the HT-polymorph has a tetragonal symmetry but crystallizes in a different space group with respect to $P4/nmm$ commonly found in other n-alkylammonium chlorides. Moreover, the doubling of the c-axis indicates the occurrence of a different packing scheme consistent with Z = 4 instead of Z = 2. Reevaluation of the pattern measured at 308 K (Figure 4) indicates the coexistence of both OAC polymorphs.

Dependence of cell parameters and volume from temperature of the HT-polymorph was investigated, in the 308 K ≤ T ≤ 473 K thermal range, by LeBail fitting (Figure 5). The volume thermal expansivity and the linear thermal expansion coefficients have been calculated applying the approach proposed in reference 30 and following the procedure described in references 31−33, using a T_r of 308 K. Results of the fitting procedure are reported in Table 2.

The a parameter expands as temperature increases, whereas the c parameter contracts. The net result is a volume expansion as the modulus of the expansivity of the a-axis is larger than that of the c-axis. It is worth noting that, from extrapolation of the volume of the HT polymorph within the stability field of the LT one, the former has a volume ca. 5.9% larger than the latter. This indicates a less efficient packing of the HT polymorph.

Besides, dependence of cell parameters and volume from temperature of the LT polymorph was evaluated. However, due to the small investigated thermal range (295 K ≤ T ≤ 303 K), only qualitative information has been extracted. In particular, a volume expansion as temperature increases has been observed. Melting starts at 463 K and is accompanied by the growing of a strong first sharp diffraction peak (FSDP) at a calculated d-spacing of ca. 21.0 Å, corresponding to Q of ca. 0.30 Å^{-1} (Figure 6). The FSDP d-spacing is significantly shorter than that of the long 020 reflection, which is of ca. 23 Å at 473 K (Δ ca. 8.7%). FSDP has a very weak third-order companion at Q ca. 0.90 (0.30 × 3) Å^{-1}. The intensity of FSDP increases up to a maximum value at 478 K and subsequently decreases as temperature increases indicating the progressive lost of correlation within the melt. Slow cooling to RT of the melt produces a well-crystallized, albeit microcrystalline, LT polymorph. The persistence of a very weak FSDP at RT indicates an incomplete recrystallization of the melt.

Crystal Polymorphism of DAC. By evaluation of the full data set (Figure 7), two phase transitions have been detected at 318 K (T_{d1}) and at 323 K (T_{d2}), respectively, in qualitative agreement with reference data.[13]

Therefore, the stability field of the LT monoclinic polymorph is very limited in the investigated thermal range (three data points). According to the few experimentally accessible points, it is not possible to describe with accuracy the variation of both cell parameters and crystal structure as a function of temperature. However, as a general trend, b and c cell parameters expand as temperature increases as well as the monoclinic β angle. Instead, the a-parameter is substantially unaffected by heating. Besides, Rietveld refinements, carried out from nonambient data, do not show any appreciable difference with respect to the RT structure. At T_{d1}, the LT polymorph coexists with a new-formed phase. At T_{d2}, the LT polymorph is replaced by a further polymorphic modification of DAC that becomes the only one at 328 K. This second phase transition signals the occurrence of a phase structurally related to the LT polymorph of HeAC. In fact, autoindexing returned a solution in the tetragonal crystal system for cell parameters a of ca. 5.00 Å and c of ca. 28.5 Å. Dependence of cell parameters and volume from temperature (Figure 8) was investigated by LeBail fitting that pointed out to extinction conditions consistent with the same $P4/nmm$ space group of the LT polymorph of HeAC.

The volume thermal expansivity and the linear thermal expansion coefficients have been calculated for the HT-polymorph following the same procedure adopted for HT-OAC using a T_r of 328 K. Results of the fitting procedure are reported in Table 3.

It is evident that the dependence of cell parameters and volume in both tetragonal polymorphic forms of HeAC and DAC follows a similar behavior. In fact, the a-parameter expands, whereas the c-parameter contracts as temperature

dx.doi.org/10.1021/jp403103w | J. Phys. Chem. B 2013, 117, 7806−7818

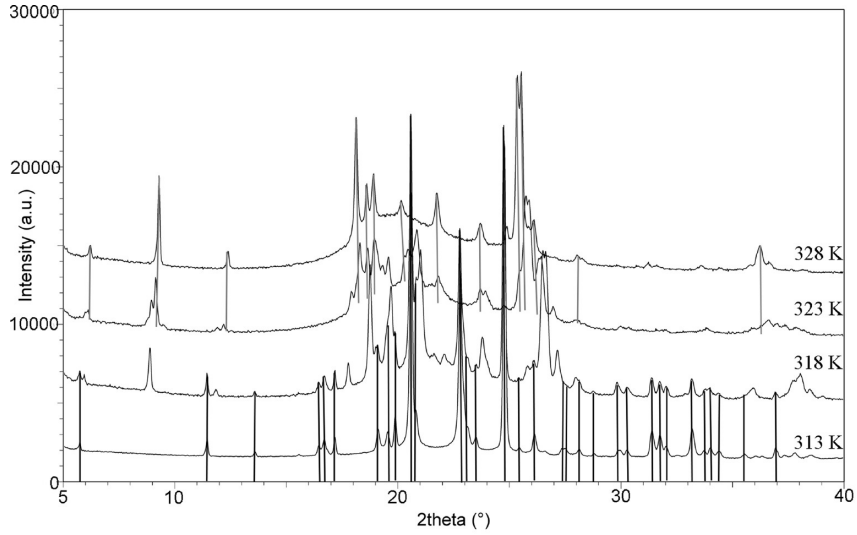

Figure 7. Magnified view of the diffraction patterns measured in the 313 K < T < 328 K thermal range. Black bars indicate the position of the Bragg reflections of the DAC LT-polymorph, whereas gray bars indicate the positions of the Bragg reflections of the DAC HT-polymorph. Diffraction patterns are vertically displaced for clarity.

increases as well. Comparison of the corresponding a_0 linear expansion coefficients indicates that DAC expands more than HeAC. This behavior results from a combined larger expansion of the a-parameter and a larger contraction of the c-parameter of DAC as compared to HeAC. This could be due to a more relevant bending or kinking with respect to the 4-fold axis of the aliphatic chain of DAC with respect to HeAC.

Melting starts at 458 K and is accompanied, similarly to OAC, by the growing of a strong FSDP at a calculated d-spacing of ca. 24.8 Å, corresponding to Q of ca. 0.26 $Å^{-1}$ (Figure 9). FSDP has a weaker third-order companion at Q ca. 0.78 (0.26 × 3) $Å^{-1}$. As in the case of OAC, the d-spacing is shorter (Δ ca. 8.1%) than the fully elongated c-parameter, ca. 27 Å, of the HT-polymorph as calculated just before melting (Figure 8a).

As far as the intermediate phase, occurring in the narrow 318 K ≤ T ≤ 323 K thermal range, is concerned, structure characterization has been very challenging. Despite the relevant number of attempts to index the pattern, it was impossible to obtain a meaningful solution.

In order to corroborate our findings, and assess analogies and/or differences, it would have been meaningful to perform some XRD measurements on compounds that share most of the chemical topology with the monoalkylammonium chlorides reported in this work, like, for instance, the analogous monoalkylphosphonium salts. Unfortunately, these compounds are neither commercially available nor easily obtainable by synthesis, therefore we cannot report any data in the present manuscript, but we hope to be able to study these systems in the near future.

The results of the parallel calorimetric study by DSC are collected in Figure 10. The curves of OAC and DAC are reported. Two main endothermic transitions are present in all the samples, the first one in the temperature range 303−348 K, and the second one in the temperature range 453−498 K.

For each process, the related ΔH and peak characteristic temperature are collected in Table 4. The DSC traces show and confirm the characteristic temperature of the polymorphic phase transitions. In Figure 10, it can be noted that for DAC only one process is present, but the zoomed-in box clearly enhances the overlapping of two main peaks that are not fully resolved. This effect can be mainly due to a mass-effect, since a higher amount of sample is required with respect to the diffraction technique. The corresponding ΔH value is the sum of the two processes. In addition, the scanning temperature tends to shift the peak maximum by a few degrees. The same effect can be noted for the melting peaks that are slightly shifted to higher temperatures.

The attempt to lower the scanning rate below 1 K min^{-1}, to be closer to the diffraction conditions, gave very broad peaks with consequent higher errors in the ΔH calculations.

Structural Properties of OAC/Water and DAC/Water Mixtures. The experimental X-ray diffraction patterns and Diff(r) functions of the OAC/water and DAC/water mixtures are shown as a dotted black line in Figure 11. The $I(Q)$'s are very similar to each other and are constituted by a principal double peak, whose peak positions are found at about 2.09−2.11 and 2.92 $Å^{-1}$, followed by two less intense peaks centered at 4.85 and 7.18−7.33 $Å^{-1}$, and some less well-defined oscillations beyond. The Diff(r) functions of the two mixtures also show a very similar trend, being characterized by three main peaks, centered at about 2.90, 4.50, and 6.85 Å for OAC and at 2.90, 4.60, and 6.95 Å, for DAC. As already observed for the mixtures with water of alkylammmonium chlorides with shorter alkyl chains,[7−9] the main contributions to the first peak of the Diff(r) functions originate from contacts between the chloride ion and the oxygen atoms of water molecules belonging to the Cl^- first coordination sphere, and from oxygen−oxygen interactions between nearest neighbor water molecules. In particular, the latter contribution is dominant in highly diluted mixtures like those investigated here.

The X-ray diffraction experimental data have been used to validate the structural results obtained from MD. To this end, MD simulations of the OAC/water and DAC/water mixtures have been carried out using the computational setup described in the Experimental Section, and a theoretical $I(Q)$ and Diff(r) functions have been calculated, for each investigated system, from the MD trajectories. The theoretical structure factors are compared with the experimental ones in Figure 11a and 11c for OAC and DAC, respectively. The experimental pattern of peak

dx.doi.org/10.1021/jp403103w | J. Phys. Chem. B 2013, 117, 7806−7818

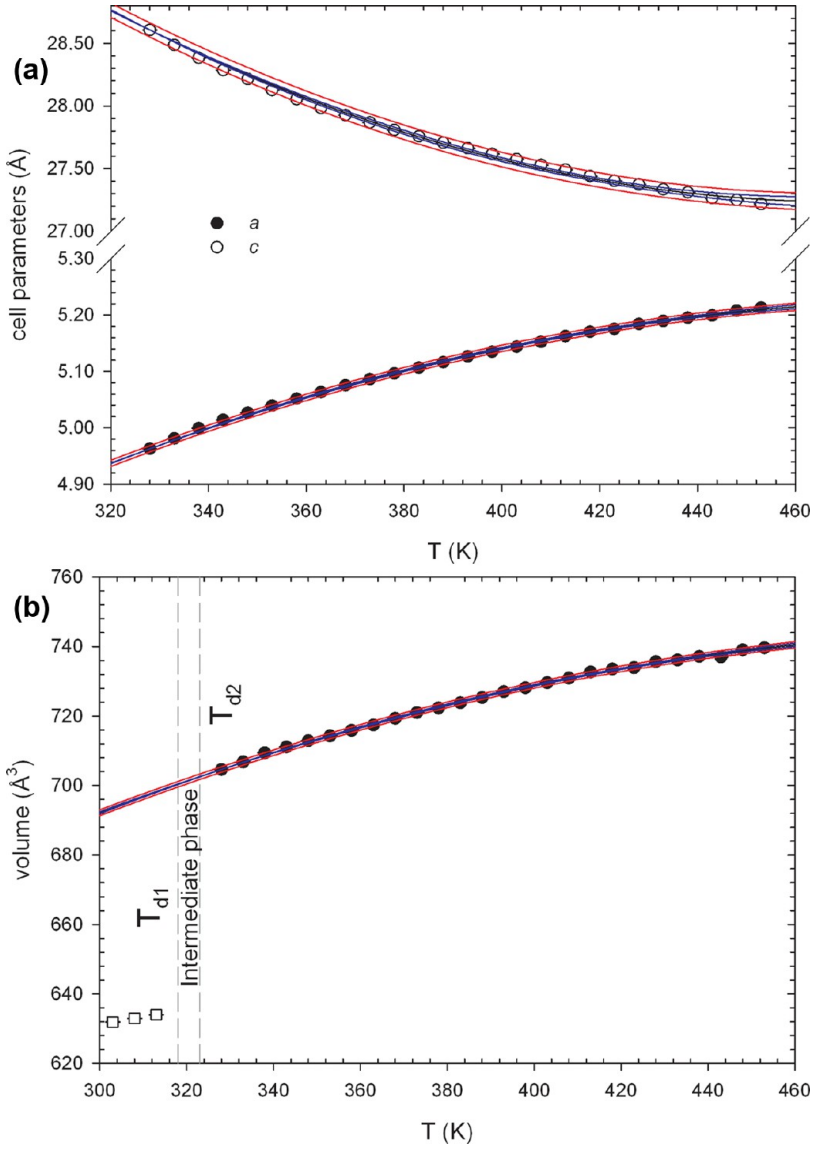

Figure 8. Evolution of cell parameters and volume with temperature for the HT polymorph of DAC: (a) cell parameters; (b) volume. Volume data of the LT polymorph are reported for comparison. Fitting of the expression $\alpha_V(T) = a_0 + a_1T$ (see below), confidence (95% level), and prediction intervals are reported. Vertical dashed gray lines indicate temperatures at which the two phase transitions occur.

positions and intensities is well reproduced by the theoretical $I(Q)$'s for both mixtures, the agreement being almost perfect in the case of DAC. A similar result has been obtained in distance space. As it can be seen from the comparison shown in Figure 11b and 11d, also in this case a very good agreement between the theoretical and experimental Diff(r)'s has been found for the two studied mixtures.

As described in the Methods section, MD simulations have been carried out using standard force fields reported in the literature to describe all of the interactions among the atoms of the systems, with the exception of one Lennard-Jones parameter for the Cl−water interaction ($\sigma_{Cl\text{-}OW}$, where OW is the oxygen atom of the water molecule), for which the value previously optimized for the EAC/water mixture was employed.[7] In our previous works on PAC/water[8] and HeAC/water[9] mixtures, by using the same $\sigma_{Cl\text{-}OW}$ parameter it was possible to obtain a very good agreement between the theoretical and experimental diffraction patterns. These results, together with the good agreement between theory and experiment obtained in the present work, indicate that the force field parameter refined for EAC is able to correctly describe the structural properties of alkylammonium chlorides regardless of the length of the alkyl chain, and also in conditions of water concentration very different from those used for the force field refinement.[7]

Once the reliability of the MD structural results has been established, the structural properties of the systems can be investigated by analyzing the trajectories. Structural arrangements of water molecules around the chloride ion are characterized by the Cl−OW and Cl−HW radial distribution functions, where OW and HW are the oxygen and hydrogen atoms of water molecules, respectively. The results obtained from the MD trajectories are shown in Figure 12a. The Cl−OW and Cl−HW $g(r)$'s calculated from the simulations of OAC/water and DAC/water mixtures are very similar. Moreover, the $g(r)$'s show very sharp and distinct first peaks, located at 3.07 and 2.15 Å (oxygen and hydrogen atom, respectively) meaning that strong anion−water interactions are

dx.doi.org/10.1021/jp403103w | J. Phys. Chem. B 2013, 117, 7806−7818

Table 3. Linear and Volume Thermal Expansion Coefficients a_0 and a_1 of High Temperature DAC Calculated Using a Reference Temperature T_r of 328 K[a]

		low-temperature HeAC	high-temperature DAC
		303 K < T < 478 K	328 K < T < 453 K
a-parameter	R^2	0.9977	0.9988
	a_0 ($\times 10^{-6}$)	361(4)	636(6)
	a_1 ($\times 10^{-8}$)	−65(3)	−191(6)
	a_{Tr}	5.00483(5)	4.96287(12)
c-parameter	R^2	0.9952	0.9958
	a_0 ($\times 10^{-6}$)	−252(4)	−671(10)
	a_1 ($\times 10^{-8}$)	52(3)	23(10)
	c_{Tr}	19.4495(4)	28.6068(13)
V	R^2	0.9908	0.9988
	a_0 ($\times 10^{-6}$)	468(11)	588(6)
	a_1 ($\times 10^{-8}$)	−79(8)	−154(6)
	V_{Tr}	487.176(17)	704.59(5)

[a]Data of low-temperature HeAC[9] are reported for comparison.

present in the mixtures, as previously observed also for the lower homologues of the alkylammonium chlorides family.[7−9] The average number of water molecules in the Cl^- first coordination sphere has been calculated by integrating the Cl−OW $g(r)$ up to the first minimum (3.76 Å). The coordination numbers obtained are 7.05 and 6.53 for OAC/water and DAC/water mixture, respectively. Both values fall within the experimental range predicted for the Cl^- ion in aqueous solution (5−11 with a strong preference for 6).[34]

Another interesting feature that emerges from the Cl−water $g(r)$ analysis is the presence of two first shell peaks in the Cl−HW $g(r)$'s, the former at shorter distances and the latter at longer distances as compared to the Cl−OW $g(r)$ first maximum, indicating that the first shell water molecules orient only one hydrogen atom toward Cl^-, due to the strong ability of the Cl^- ion to form hydrogen bonds, as also shown for other halide ions in aqueous solution.[34,35] The presence of highly directional hydrogen bonds between the anion and the water molecules belonging to its first hydration shell can be inferred by calculating the distribution function of the ω angles (Figure 12c). In both mixtures, the ω distributions are almost coincident and are in line with the distributions previously obtained for halide ions in aqueous solution.[35] The ω functions are characterized by a sharp peak located at 0°, indicating that one hydrogen atom of the first shell water molecules is strongly bound to the anion in a linear Cl···H−O configuration. The second hydrogen atom, which has a larger rotational freedom, gives rise to a second peak which is less intense and much broader than the first one, whose maximum is found at about 102°.

The geometry of the Cl^- first hydration shell can be evaluated by the analysis of the angular distribution functions of O−Cl−O ψ angle, plotted in Figure 12d. The ψ distributions obtained from the two trajectories drop to zero for 1 − cos ψ values lower than 0.25, showing that ψ angles smaller than 41° are prohibited in both simulations. Moreover, two broad peaks are found at ψ = 70° and ψ = 142° for the OAC/water mixture, and at ψ = 71° and ψ = 146° for DAC, and the functions are similar to those previously obtained from a MD simulation of the Br^- ion in aqueous solution.[35] The analysis of ψ angles for ions forming very stable first hydration spheres in aqueous solution, such as the divalent or trivalent cations, gives ψ distributions with much sharper and narrower peaks than those obtained in the present case,[36−39] indicating the presence of strong hydration complexes with specific symmetry. On the contrary, the broad peaks found here for the Cl^- ion suggest the existence of a much more unstructured and disordered first coordination sphere, where it is not possible to single out a particular symmetry of the shell. This is because halide−water interactions are usually weaker than the interactions with water of divalent or trivalent cations.

In order to gain additional insights into the structural properties of the OAC and DAC/water mixtures, the $g(r)$'s of a selected subset of atoms have been computed from MD trajectories (see Figure 13). A series of coordination numbers

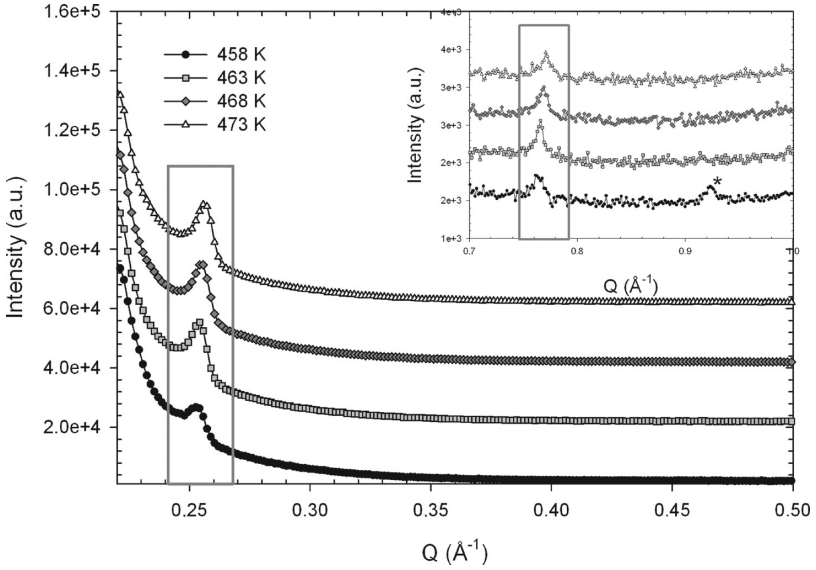

Figure 9. Evolution of FSDP of DAC, located at Q ca. 0.26 Å^{-1}, from 458 to 473 K. Inset: evolution of the third-order FSDP at Q ca. 0.78 (0.26 × 3) Å^{-1}. Star marks the position of the 004 reflection of HT-DAC arising from incomplete melting at 458 K. Diffraction patterns have been displaced vertically for clarity.

dx.doi.org/10.1021/jp403103w | J. Phys. Chem. B 2013, 117, 7806−7818

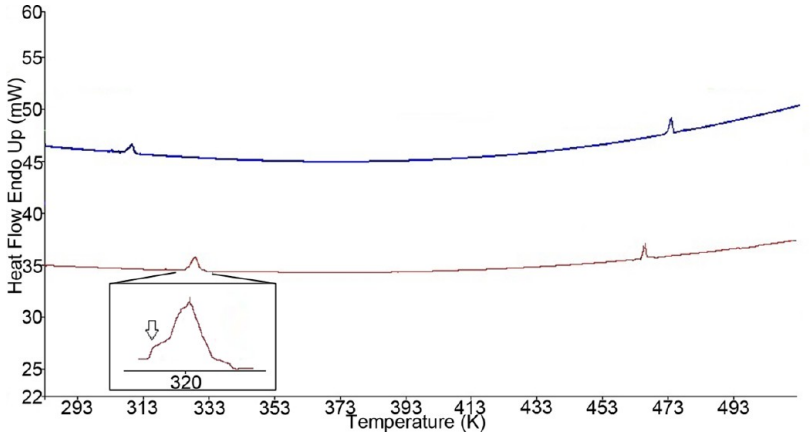

Figure 10. DSC curves of OAC and DAC. The zoomed-in box is related to the DAC first process.

Table 4. Calculated Characteristic Peak Temperatures and ΔH for the OAC and DAC Samples

	peak K	ΔH J/g	peak K	ΔH J/g
OAC	307.1	6.79	474.0	45.80
DAC	326.7[a]	107.17[a]	465.8	51.61

[a]Sum of the two overlapped processes for DAC.

were also calculated by integrating the $g(r)$'s up to a certain cutoff distance, chosen as the position of the first minimum of the corresponding radial distribution function. Selected $g(r)$ first peak distances are reported in Table 5, together with the computed coordination numbers and cutoff values used in the calculations.

The N−OW and N−HW $g(r)$'s calculated from the two simulations (Figure 13a) show the existence of a first hydration shell of water molecules around the N atom of the cation, but the peaks are less pronounced as compared to the Cl−water $g(r)$'s, as cation−water interactions are weaker than the anion−water ones. The first shell water molecules tend to orient the oxygen atom toward the N atom, but the oxygen and hydrogen $g(r)$ first peaks are not well separated, and a larger orientational freedom is found, as compared to the Cl^- first hydration shell. As far as the carbon atom of the terminal methyl group (CT) is concerned, the presence of a peak at about 4 Å in the CT−CT $g(r)$ (Figure 13b) indicates that the cation alkyl chains aggregate to some extent in OAC/water and DAC/water mixtures, the aggregation being more pronounced in the case of DAC, as evidenced by the higher CT−CT coordination number reported in Table 5. However, the alkyl chains are not completely segregated in the hydrophobic domain, as highlighted by the presence of CT−OW interactions in both the investigated mixtures (Figure 13c). Note that the CT−OW and CT−HW $g(r)$ first peaks calculated from the simulation of the DAC/water mixture have a lower intensity, and the CT−

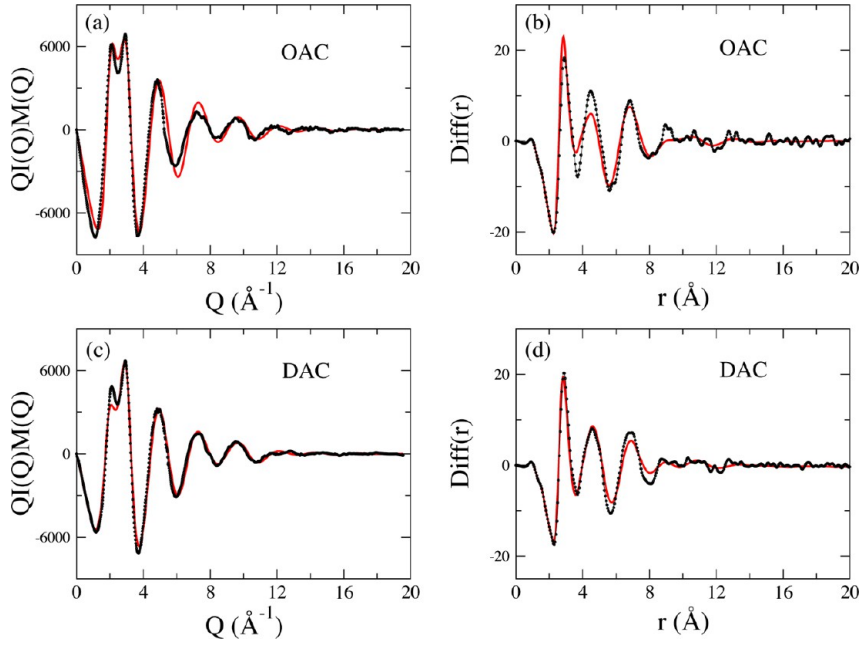

Figure 11. Comparison between the experimental structure factors (dotted black line) of the OAC/water (a) and DAC/water (c) mixtures, and the theoretical structure factors (solid red line) calculated from the corresponding MD simulations. Comparison between the experimental Diff(r) functions (dotted black line) of the OAC/water (b) and DAC/water (d) mixtures, and the theoretical Diff(r)'s (solid red line) calculated from the corresponding MD simulations.

dx.doi.org/10.1021/jp403103w | J. Phys. Chem. B 2013, 117, 7806−7818

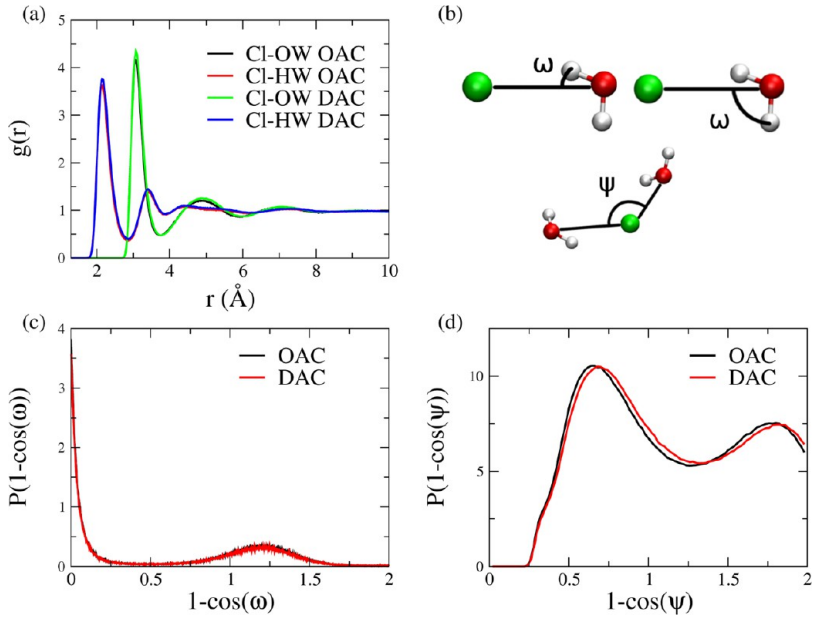

Figure 12. (a) Cl−OW and Cl−HW radial distribution functions calculated from the MD simulations of the OAC/water and DAC/water mixtures. OW and HW are the oxygen and hydrogen atoms of the water molecules. (b) Definition of the ω and ψ angles. (c) ω angular distribution functions calculated from the MD simulations of the OAC/water (black line) and DAC/water mixtures (red line). (d) OW−Cl−OW ψ angular distribution functions calculated from the MD simulations of the OAC/water (black line) and DAC/water (red line) mixtures.

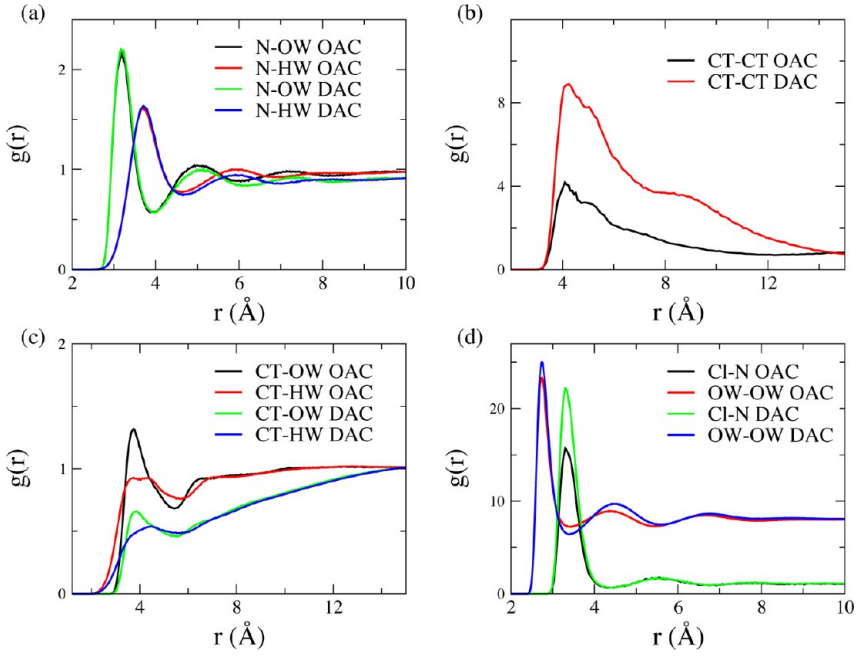

Figure 13. Radial distribution functions $g(r)$'s calculated from the MD simulations of the OAC/water and DAC/water mixtures. (a) N−OW and N−HW $g(r)$'s. (b) CT−CT $g(r)$'s. CT is the C atom of the terminal methyl group. (c) CT−OW and CT−HW $g(r)$'s. (d) OW−OW and Cl−N $g(r)$'s. The OW−OW $g(r)$'s are shown multiplied by a factor of 8 for the sake of clarity.

OW coordination number is significantly lower (see Table 5) as compared to the OAC one. The lower number of water molecules that are found in the proximity of the methyl group can be explained by the increased aggregation of the alkyl chains in the DAC/water mixture. Moreover, the high and well-defined short-range peak of the OW−OW $g(r)$ (Figure 13d) indicates that water molecules in the mixtures aggregate and form water clusters.

A very interesting result that emerged from our previous results on HeAC/water mixtures was that cations and anions tend to interact with each other also in conditions of very high dilution.[9] This proves to also be the case for OAC/water and DAC/water mixtures, as evidenced by the strong Cl−N correlation that is found in both simulations (Figure 13d). The Cl−N coordination numbers reported in Table 5 show that this interaction is significant, albeit the great excess of water present in the mixtures. Additional insights into this behavior can be gained by defining an instantaneous anion−cation coordination number as the number of N atoms at a distance from the Cl^- ion shorter than the Cl−N g(r) first

dx.doi.org/10.1021/jp403103w | J. Phys. Chem. B 2013, 117, 7806−7818

Table 5. Structural Parameters of the Radial Distribution Functions $g(r)$'s Depicted in Figure 13 Calculated from the MD Simulations of the OAC/Water and DAC/Water Mixtures[a]

	R(Å)		N		
	OAC	DAC	OAC	DAC	cutoff distance (Å)
N−OW	3.20	3.20	6.15	5.60	3.93
CT−CT	4.10	4.20	1.18	2.75	7.50
CT−OW	3.74	3.86	16.0	8.30	5.50
Cl−N	3.30	3.32	0.40	0.52	4.41
OW−OW	2.74	2.74	4.75	4.31	3.40

[a] R is the position of the $g(r)$ first peak, and N is the coordination number calculated by integration of the corresponding $g(r)$. The cutoff distances used in the calculation of N are also reported.

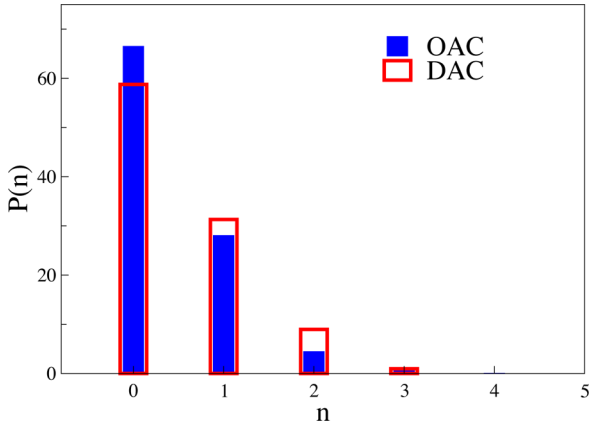

Figure 14. Instantaneous cation−anion coordination number (n) distribution, expressed in percentage, obtained from the MD simulations of the OAC/water (filled blue bars) and DAC/water (open red bars) mixtures.

minimum, and analyzing its variation along the trajectories (see Figure 14). The results of this analysis show that in both OAC/water and DAC/water mixtures the most probable ion configuration are 0-coordinated species. However, a significant percentage of anions (about 30%) are coordinated to one cation, and there is also a non-negligible percentage of anions that simultaneously coordinate two cations. All together, these results indicate that cations and anions do not possess a completely closed hydration shell, but rather, "solvent-shared ion pairs" are formed, in which one or more water molecules belonging to the anion first hydration sphere can be shared with the N atom of the cation. This is in perfect line with our previous findings on mixtures with water of the lower homologues of the alkylammonium chlorides family,[7−9] where we have put in evidence the existence of these "solvent-shared ion pairs", and we have shown that the ion pairs were able to also survive in conditions of very high concentrations of water molecules.[9]

CONCLUSIONS

The analysis of the thermal behavior of OAC and DAC has provided relevant new information. OAC shows a polymorphic phase transition that starts at 308 K and is completed at 313 K. No further structural modifications were observed up to the melting temperature. The LT (T < 308 K) structural modification is monoclinic a = 25.5771(4) Å, b = 4.72090(5) Å, c = 9.39663(10) Å, β = 97.8549(15)°, volume 1123.97(6) Å^3, Z = 4, $P2_1/c$ possible space group. Besides, the HT polymorph is tetragonal a = 5.10074(6) Å, c = 47.1860(22) Å, volume 1227.67(6) Å^3, Z = 4, $P4_2/n$ possible space group. This is a different space group with respect to $P4/nmm$ commonly found in other n-alkylammonium chlorides. Moreover, the doubling of the c-axis indicates the occurrence of a different packing scheme consistent with Z = 4 instead of Z = 2. Due to the small accessible thermal range for the LT polymorph, the volume thermal expansivity and the linear thermal expansion coefficients have been calculated for the HT modification only.

HT-OAC shows a volume expansion arising from the combined effect of the a parameter and the c parameter contraction as temperature increases. In fact, the modulus of the expansivity of the a-axis is larger than that of the c-axis. From extrapolation of the volume of the HT polymorph within the stability field of the LT one, it is apparent that the former has a volume ca. 5.9% larger than the latter. Melting starts at 463 K and is accompanied by the growing of a strong FSDP occurring at a d-spacing of *ca.* 21.0 Å, which is significantly shorter than that of the long 020 reflection, which is of ca. 23 Å at 473 K. The intensity of FSDP reaches a maximum value at 478 K and subsequently decreases as temperature increases, signaling the progressive lost of correlation within the melt.

The thermal behavior of DAC is more complex than that of OAC. Two phase transitions have been detected at 318 (T_{d1}) and 323 K (T_{d2}). At T_{d1}, the LT polymorph coexists with a new-formed phase. At T_{d2} the LT polymorph is replaced by a further polymorphic modification of DAC that becomes the only one at 328 K. This second phase transition signals the occurrence of a phase, closely related to the LT polymorph of HeAC, that crystallizes in the tetragonal crystal system a = *ca.* 5.00 Å and c = *ca.* 28.5 Å, $P4/nmm$ space group. The dependence of cell parameters and volume in both tetragonal polymorphic forms of HeAC and DAC follows a similar behavior: an expansion of the a-parameter and a contraction of the c-parameter as temperature increases. Additionally, DAC expands more than HeAC. This behavior has been explained as arising from a more relevant bending or kinking with respect to the 4-fold axis of the aliphatic chain of DAC with respect to HeAC. Melting starts at 458 K and is accompanied, similarly to OAC, by the occurrence of a very intense FSDP at a d-spacing of ca. 24.8 Å. Similarly to OAC, the d-spacing is shorter than the fully elongated c-parameter of the HT-polymorph as calculated just before melting.

The origin of FSDP has been recently reviewed.[40] Their presence has been related to the occurrence of highly structured domains,[41−43] but such connection has been recently questioned.[44] In fact, FSDP occurrence has been linked to the second coordination shell of the ions along the vector of alkyl-chain substituents in Im_{n1}^+ cations.[44] According to the linear shift of FSDP with the alkyl chain length n, it has been hypothesized that such behavior is due to the increase of volume from the ion-polar substituents.[44] In effect, EAC, OAC, and DAC show a linear shift of FSDP as a function of n as well. However, an investigation of alkylammonium chloride characterized by longer alkyl chains is required to confirm such behavior. We are currently undertaking a study regarding compounds with n = 12 and 18.

In addition, the structural properties of OAC/water and DAC/water mixtures have been studied using a combined MD and X-ray diffraction approach. In particular, the X-ray diffraction experimental data have been used to validate the structural results obtained from the MD simulations, and a very

dx.doi.org/10.1021/jp403103w | J. Phys. Chem. B 2013, 117, 7806−7818

good agreement between the theoretical and experimental diffraction patterns has been obtained for both investigated mixtures. A thorough analysis of the MD trajectories has been carried out, showing that strong anion−water interactions are present in the mixtures and about 7 water molecules are bound to chlorine ion with a linear Cl···H−O hydrogen bond, giving rise to a rather unstructured and disordered first hydration shell. The cation alkyl chains aggregate to some extent in OAC/water and DAC/water mixtures, but the alkyl chains are not completely segregated in the hydrophobic domain, and the carbon atom of the terminal methyl group also interacts with the water molecules present in the mixtures. A very interesting result that emerged from the MD analysis is that cations and anions tend to interact with each other albeit the great excess of water present in the mixtures, by forming "solvent-shared ion pairs", in which one or more water molecules are shared between Cl^- and the alkylammonium cation. This is in line with our previous results on aqueous solutions of the lower homologues of the alkylammonium chlorides family.[7−9] Therefore, the existence of "solvent-shared ion pairs" seems to be a peculiar characteristics of these complex systems.

AUTHOR INFORMATION

Corresponding Author

*E-mail: valentina.migliorati@uniroma1.it (V.M.); paolo.ballirano@uniroma1.it (P.B.)

Notes

The authors declare no competing financial interest.

ACKNOWLEDGMENTS

This work was supported by the University of Rome la Sapienza (Prin 2009 Caminiti (2009WHPHRH). V.M. acknowledges financial support from Ateneo 2011-Bodo; L.G. acknowledges financial support from "FIRB" Futuro in Ricerca (RBFR086BOQ_001, Structure and dynamics of ionic liquids).

REFERENCES

(1) Rogers, R. D.; Seddon, K. R. *Science* **2003**, *302*, 792.
(2) D'Angelo, P.; Zitolo, A.; Migliorati, V.; Bodo, E.; Aquilanti, G.; Hazemann, J. L.; Testemale, D.; Mancini, G.; Caminiti, R. *J. Chem. Phys.* **2011**, *135*, 074505.
(3) Gontrani, L.; Bodo, E.; Triolo, A.; Leonelli, F.; D'Angelo, P.; Migliorati, V.; Caminiti, R. *J. Phys. Chem. B* **2012**, *116*, 13024.
(4) Kohagen, M.; Brehm, M.; Thar, J.; Zhao, W.; Muller-Plathe, F.; Kirchner, B. *J. Phys. Chem. B* **2011**, *115*, 693.
(5) Zabinska, G.; Drozdowska, G.; Kisza, A.; Ferloni, P. *J. Chem. Eng. Data* **1998**, *43*, 562.
(6) Zabinska, G.; Urbaniak, G.; Kisza, A.; Ferloni, P. *J. Chem. Eng. Data* **1991**, *36*, 164.
(7) Migliorati, V.; Ballirano, P.; Gontrani, L.; Triolo, A.; Caminiti, R. *J. Phys. Chem. B* **2011**, *115*, 4887.
(8) Migliorati, V.; Ballirano, P.; Gontrani, L.; Russina, O.; Caminiti, R. *J. Phys. Chem. B* **2011**, *115*, 11805.
(9) Migliorati, V.; Ballirano, P.; Gontrani, L.; Caminiti, R. *J. Phys. Chem. B* **2012**, *116*, 2104.
(10) Tsau, J.; Gilson, D. F. R. *J. Phys. Chem.* **1968**, *72*, 4082.
(11) Gilson, D. F. R.; Kertes, A. S.; Manley, R. S. J.; Tsau, J. *Can. J. Chem.* **1976**, *54*, 765.
(12) Schenk, K. J.; Chapuis, G. *Z. Kristallogr.* **1983**, *162*, 197.
(13) Schenk, K. J.; Chapuis, G. *Acta Crystallogr.* **1986**, *C42*, 1076.
(14) Kind, R.; Blinc, R.; Arend, H.; Muralt, P.; Slak, J.; Chapuis, G.; Schenk, K. J.; Zeks, B. *Phys. Rev.* **1982**, *A26*, 1816.
(15) Kong, Y.-X.; Di, Y.-Y.; Zhang, Y.-Q.; Yang, W.-W.; Tan, Z.-C. *Thermochim. Acta* **2009**, *495*, 33.
(16) Ballirano, P.; Melis, E. *Phys. Chem. Miner.* **2007**, *34*, 699.
(17) Ballirano, P.; Maras, A.; Meloni, S.; Caminiti, R. *Eur. J. Mineral.* **2001**, *13*, 985.
(18) Ballirano, P.; Sadun, C. *Struct. Chem.* **2009**, *20*, 815.
(19) Ballirano, P.; Caminiti, R. *J. Phys. Chem. A* **2009**, *113*, 7774.
(20) Caminiti, R.; Sadun, C.; Rossi, V.; Cilloco, F.; Felici, R. Italian Patent No. 01261484, 23 June 1993.
(21) (a) Carbone, M.; Caminiti, R.; Sadun, C. *J. Mater. Chem.* **1996**, *6*, 1709. (b) Abis, L.; Dell'Amico, D. B.; Busetto, C.; Calderazzo, F.; Caminiti, R.; Ciofi, C.; Garbassi, F.; Mascarelli, G. *J. Mater. Chem.* **1998**, *8*, 751. (c) Caminiti, R.; Isopo, A.; Orrù, M. A.; Albertini, V. R. *Chem. Mater.* **2000**, *12*, 369.
(22) Smith, W.; Forester, T. *J. Mol. Graphics* **1996**, *14*, 136.
(23) Jorgensen, W. L.; Ulmschneider, J. P.; Tirado-Rives, J. *J. Phys. Chem. B* **2004**, *108*, 16264.
(24) Canongia Lopes, J. N.; Pádua, A. A. H. *J. Phys. Chem. B* **2004**, *108*, 16893.
(25) Canongia Lopes, J. N.; Deschamps, J.; Pádua, A. A. H. *J. Phys. Chem. B* **2004**, *108*, 2038.
(26) Mahoney, M. W.; Jorgensen, W. L. *J. Chem. Phys.* **2000**, *112*, 8910.
(27) Pings, C. J.; Waser, J. *J. Chem. Phys.* **1968**, *48*, 3016.
(28) Coelho, A. A. *J. Appl. Crystallogr.* **2003**, *36*, 86.
(29) Bruker AXS *Topas V4.2: General Profile and Structure Analysis Software for Powder Diffraction Data*; Bruker AXS: Karlsruhe, Germany, 2009
(30) Fei, Y. Thermal expansion. In *Mineral Physics & Crystallography: A Handbook of Physical Constants, Mineral Physics and Crystallography*; Ahrens T. J., Ed.; AGU Reference Shelf 2; American Geophysical Union: Washington, DC, 1995; pp 29−44.
(31) Ballirano, P. *Phys. Chem. Miner.* **2012**, *39*, 115.
(32) Ballirano, P. *Am. Mineral.* **2012**, *97*, 1320.
(33) Ballirano, P.; Bosi, F. *Am. Mineral.* **2012**, *97*, 630.
(34) Caminiti, R.; Licheri, G.; Piccaluga, G.; Pinna, G. *J. Appl. Crystallogr.* **1979**, *12*, 34.
(35) D'Angelo, P.; Migliorati, V.; Guidoni, L. *Inorg. Chem.* **2010**, *49*, 4224.
(36) Migliorati, V.; Mancini, G.; Tatoli, S.; Zitolo, A.; Filipponi, A.; De Panfilis, S.; Di Cicco, A.; D'Angelo, P. *Inorg. Chem.* **2013**, *52*, 1141.
(37) Mancini, G.; Sanna, N.; Barone, V.; Migliorati, V.; D'Angelo, P.; Chillemi, G. *J. Phys. Chem. B* **2008**, *112*, 4694.
(38) D'Angelo, P.; Migliorati, V.; Mancini, G.; Chillemi, G. *J. Phys. Chem. A* **2008**, *112*, 11833.
(39) Migliorati, V.; Mancini, G.; Chillemi, G.; Zitolo, A.; D'Angelo, P. *J. Phys. Chem. A* **2011**, *115*, 4798.
(40) Castner, E. W., Jr.; Margulis, C. J.; Maroncelli, M.; Wishart, J. F. *Annu. Rev. Phys. Chem.* **2011**, *62*, 85.
(41) Triolo, A.; Russina, O.; Bleif, H.-J..; Di Cola, E. *J. Phys. Chem. B* **2007**, *111*, 4641.
(42) Triolo, A.; Russina, O.; Fazio, B.; Triolo, R.; Di Cola, E. *Chem. Phys. Lett.* **2008**, *457*, 362.
(43) Russina, O.; Triolo, A.; Gontrani, L.; Caminiti, R.; Xiao, D.; Hines, L. G., Jr.; Bartsch, R. A.; Quitevis, E. L.; Plechkova, N.; Seddon, K. R. *J. Phys.: Condens. Matter* **2009**, *21*, 424121.
(44) Hardacre, C.; Holbrey, J. D.; Mullan, C. L.; Youngs, T. G. A.; Bowron, D. T. *J. Chem. Phys.* **2010**, *133*, 074510.